Archives of Environmental Protection
Vol. 50 no. 4 pp. 51–63

PL ISSN 2083-4772
DOI 10.24425/aep.2024.152895

Adsorption of selected GHG on metal-organic frameworks in the context of accompanying thermal effects

Aleksandra Gajda[1], Przemysław Jodłowski[2], Katarzyna Kozieł[1], Grzegorz Kurowski[2], Kornelia Hyjek[2], Norbert Skoczylas[3], Anna Pajdak[1]*

[1]Strata Mechanics Research Institute of the Polish Academy of Sciences, Kraków, Poland
[2]Faculty of Chemical Engineering and Technology, Cracow University of Technology, Kraków, Poland
[3]AGH University of Krakow, Faculty of Geology, Geophysics and Environmental Protection, Kraków, Poland

*Corresponding author's e-mail: pajdak@imgpan.pl

Keywords: Metal-organic frameworks, CO_2 and CH_4 adsorption, isosteric heat of adsorption, thermal selectivity

Abstract: Thermal effects accompanying gas sorption on micro- and mesoporous materials provide unique insights into the type, course, and efficiency of sorption. In this study, metal-organic frameworks (MOFs) with different topologies and chemical structures were synthesized and investigated: HKUST-1, Ni-MOF-74, UiO-66, and MIL-140A. These MOFs were characterized structurally and sorptively with respect to selected greenhouse gases (GHGs). Sorption capacities for CO_2 and CH_4 were determined at several temperatures and measurement pressures, and the maximum sorption capacity was determined using the Langmuir-Freundlich model. Thermal effects accompanying adsorption were quantified through the isosteric heat of adsorption parameter. For each MOF, the values of isosteric heat of adsorption were higher for CO_2 than for CH_4. The values of this parameter was determined in the following order: HKUST-1 > Ni-MOF-74 > UiO-66 > MIL-140A. Energy homogeneity of the adsorbent surface was observed in nearly all cases, except for UiO-66 during CO_2 adsorption. Changes in the determined isosteric heat of adsorption of CO_2 with increasing sorption capacity were in the range of 5-15 kJ/mol, while for CH_4 they ranged from 1.4 to 17 kJ/mol, respectively. The level of thermal selectivity of CO_2 over CH_4 was determined in the following order: UiO-66 (1.9) > Ni-MOF-64 (1.7) > MIL-140A (1.5) > HKUST-1 (1.1).

Introduction

Greenhouse gas emissions have become a serious environmental problem. Due to rapid industrial growth and the combustion of fossil fuels, significant amounts of CO_2 are being emitted into the atmosphere. The concentration of CO_2 in the air has now reached its highest level in at least 2 million years. Since around 1750, the beginning of the Industrial Revolution, CO_2 levels have risen from 280 ppm, to 412 ppm as of 2020) (Erans et al. 2022). The capture of greenhouse gases (GHGs) has therefore become a priority, presenting scientists with new goals and challenges. The main challenge here is to develop an efficient and economically viable method for capturing these gases. Currently available methods include absorption, adsorption, membrane separation, cryogenic distillation and chemical looping combustion (Aniruddha et al. 2020, Zylka. et al. 2020). The amine absorption method uses an amine solution as an absorbent, which binds to gases through chemisorption. However, this method is energy-intensive due to regeneration of the absorbent, loss of amine through degradation and evaporation, and damage to equipment due to corrosion processes (Lin et al. 2019, Madden et al. 2019, Oschatz and Antonietti 2018, Qazvini et al. 2021). An alternative is adsorption, which has gained increasing scientific attention in recent years (Pajdak et al. 2019). Each adsorption method is based on the physical interactions between the adsorbate and adsorbent and typically follow one of the following schemes: Pressure Swing Adsorption (PSA), where the adsorbent is regenerated by changes in pressure; Vacuum Swing Adsorption (VSA), where regeneration occurs under vacuum; or Temperature Swing Adsorption (TSA), which exploits differences in the adsorbent's sorption capacity at varying temperatures (Aniruddha et al. 2020, Krzywanski et al. 2022, Tlili et al. 2009).

Metal-organic frameworks (MOFs) are a group of synthetic adsorbents with significant potential in many industrial fields. They can be used in gas separation and storage, catalysis, photocatalysis, biodetection, fuel cells, supercapacitors (Aniruddha et al. 2020, Chai et al. 2022, Czaja et al. 2009, Dhakshinamoorthy et al. 2018, Jodłowski et al. 2022, M. Li et al. 2021, Naghdi et al. 2023, Qian et al. 2020, Rieth et al. 2019, Strauss et al. 2019, Xu et al. 2020, Zhou et al. 2021). MOFs have a unique structure, which results in their low weight, high porosity and exceptional sorption capacity, and specific surface

area (Aniruddha et al. 2020, Mahdipoor et al. 2021, Valverde et al. 2021). The crystalline three-dimensional structure of MOFs consists of metal centers and organic ligands (Furukawa et al. 2013, Strauss et al. 2019). Their modular structure enables the creation of an infinite number of coordination polymers and allows for post-synthetic modification (Furukawa et al. 2013). This characteristic distinguishes MOFs from other known and commonly used adsorbents such as activated carbon, porous silica or zeolites. Moreover, MOFs can be tailored for specific applications by selecting the appropriate synthesis method and performing chemical modifications. These factors contribute to their superiority over other adsorbents and uniqueness (Lee et al. 2013, H. Li et al. 2019).

An effective adsorbent should be as inexpensive as possible to produce and to regenerate. Most importantly, it should have a high sorption capacity, selectivity for the chosen adsorbate, and exhibit strong mechanical, thermal, and chemical durability (Czarnota et al. 2019, Ding et al. 2019, Gargiulo et al. 2020, Kong and Li 2021). MOFs can be synthesized through various methods, including solvothermal synthesis, microwave-assisted solvothermal synthesis, electrochemical synthesis, sonochemical synthesis, mechanochemical synthesis, microfluidic synthesis, ionothermal synthesis, and dry-gel conversion synthesis (Aniruddha et al. 2020, Lee et al. 2013). While MOFs are expensive to produce due to the high cost of substrates (Elhenawy et al. 2020), their advantages far outweigh this disadvantage. In terms of CO_2 sorption efficiency, MOFs are far superior to other adsorbents. They exhibit higher working capacity for CO_2 compared to liquid amines, ionic liquids, zeolites, hybrid ultraporous materials (HUMs), soda lime, or amine-functionalized inorganics (Elhenawy et al. 2020). The high potential of MOFs for gas capture is influenced by their structural properties, such as specific surface area, porosity, average pore size and pore size distribution (Becker et al. 2017, Carreon and Venna 2020, Choi et al. 2017, D. Li et al. 2021, H. Li et al. 2019, Mangal et al. 2018, Nuhnen and Janiak, 2020, Strauss et al. 2019, Xiao and Liu 2019). Equally important is the interaction potential between the gas molecules and the MOF surface. In some cases, intermolecular interactions can be so strong that they become the dominant factor influencing the sorption process.

Adsorption on MOFs occurs according to molecular sieving theory, where particles with the appropriate kinetic diameter are adsorbed (Elhenawy et al. 2020). Most MOFs have a high affinity for acidic gases, particularly CO_2 (Aniruddha et al. 2020), which is a key aspect in the context of CO_2 capture from gas mixtures. Many studies have been dedicated to determining the sorption efficiency of MOFs for CO_2 and CH_4, relative to their structural analysis (Abdelnaby et al. 2024, Bisotti et al. 2024, Furukawa et al. 2013, Jodłowski et al. 2022, Mason et al. 2014, Senkovska and Kaskel 2008). The effect of adding functional groups and ions on sorption has been studied, though with varying results. This is because these modifications often clog the access pathways for gases into the pores, which is typically accompanied by a decrease in sorption capacity (Rieth et al. 2019). On the other hand, a positive effect was achieved by introducing defects into the surface structure, such as removing individual linkers and opening access pathways directly to metallic centers (Kurzydym and Czekaj 2020, H. Li et al. 2019).

High selectivity for a particular gas is clearly of practical use. Selectivity reflects the adsorbent's preference for a specific adsorbate, which is important when using adsorbents to capture a particular component from gas mixtures. Numerous studies in the literature investigate the selectivity of MOFs for gases (D. Li et al. 2021, H. Li et al. 2019). Chowdhury et al. (Chowdhury et al. 2012) studied HKUST-1-type MOFs at a pressure of 200 kPa and a temperature of 296 K, achieving a CO_2/CH_4 selectivity of 7.4 and a CO_2 sorption capacity of 5.27 mmol/g. The high selectivity of CO_2 over CH_4 in Ni-MOF-74 and UiO-66 makes these MOFs suitable for purifying natural gas from carbon dioxide. HKUST-1, however, is less effective in this regard, as its CO_2 capture efficiency is much lower. Rafati Jolodar et al. (Rafati Jolodar et al. 2024) conducted a study on natural gas purification from CO_2 using MIL-101(Cr-Al) as an example.

Many MOFs exhibit high thermal stability within the temperature range of 523-773 K. Their resistance to high temperatures is due to the presence of strong bonds in their structure, such as carbon-carbon, carbon-oxygen, and carbon-hydrogen bonds (Furukawa et al. 2013). However, the factors determining MOF stability are not fully understood (Rieth et al. 2019). Some MOFs show high chemical stability, while others degrade easily in the presence of moisture (Canivet et al. 2014). Park et al. (K. S. Park et al. 2006) demonstrated the high chemical stability of ZIF-8, which retained its structure after immersion in boiling benzene, methanol and water for 7 days. However, in a similar test using an 8-mol NaOH solution, ZIF-8 lost its properties after 24 h.

One of the key parameters for a comprehensive interpretation of adsorption processes and adsorbate-adsorbent interactions is the isosteric heat of adsorption. This parameter determines the average binding energy of a fluid molecule adsorbed at a specific coverage of the adsorbent surface (Mason et al. 2014). It helps identify the type of adsorption, distinguishing between weak physisorption and strong chemisorption (Nuhnen and Janiak 2020). This is particularly important in the search for adsorbents that enable efficient capture of greenhouse gases (GHGs), especially CO_2. Park et al. (H. J. Park and Suh 2013) used this parameter to characterize interactions between the SNU-100 MOF and CO_2. Different metal cations were implanted into the pore space of the MOF to optimize SNU-100 for the most effective CO_2 capture. Mahdipoor et al. (Mahdipoor et al. 2021) studied CO_2 sorption by MIL-101(Fe) and MIL-101(Fe)-NH_2 at temperatures of 291 K and 303 K and pressures up to 4 MPa. For the same sorption capacity, they observed a difference of 10.1 kJ/mol in the isosteric heat of adsorption between the two MOFs, indicating that, in addition to physisorption, CO_2 chemisorption significantly influences the adsorption mechanism. Knowledge of the isosteric heat of adsorption also allows for characterizing the heterogeneity of an adsorbent's energy, helping to distinguish between homogeneous and heterogeneous adsorbents (Cimino et al. 2017). Yulia et al. (Yulia et al. 2019) conducted CO_2 sorption studies on MIL-101(Cr) at three temperatures (298, 300, 308 K) and pressures up to 600 kPa. They fitted a Thoth model to the sorption data and calculated the isosteric heat of adsorption. Based on the variation of this heat with adsorbate occupancy, they deduced a high degree of heterogeneity in the surface structure of MIL-101(Cr). The isosteric heat of adsorption is

also used to determine the heat of condensation in mesoporous adsorbents (Neimark et al. 1998, Olivier 2000).

The purpose of this article is to highlight the importance and innovation of using MOFs for CO_2 and CH_4 capture, and to comprehensively characterize selected MOF compounds, with a special focus on the thermal effects associated with adsorption. The authors of the article synthesized four types of MOFs, which they structurally and sorptively characterized in relation to CO_2 and CH_4, paying particular attention to the isosteric heat of sorption. They then compared their results with values reported in the literature.

Materials

Among the numerous types of MOF structures differing in chemical composition and topology, the following were selected for study: (1) HKUST-1, a copper-based metal-organic framework with 1,3,5-benzenetricarboxylic acid ligands in between (Hong Kong University of Science and Technology); (2) Ni-MOF-74, a framework consisting of nickel clusters linked to 2,5-dihydroxyterephthalic acid ligands; (3) UiO-66, a zirconium-based metal-organic framework composed of $[Zr_6O_4(OH)_4]$ octahedra and 1,4-benzenedicarboxylic acid ligands (Universitetet i Oslo); and (4) MIL-140A, consisting of zirconium clusters linked by 1,4-benzenedicarboxylic acid ligands of the formula $[ZrO(O_2CC_6H_4CO_2)]$ (Matériaux de l'Institut Lavoisier). All types of MOF structures studied were synthesized at the Cracow University of Technology, Faculty of Chemical Engineering and Technology.

Synthesis

HKUST-1 was synthesized in accordance with the procedure described elsewhere (Bordiga et al. 2007), with some modifications. A total of 2.9 mmol of copper (II) nitrate trihydrate was dissolved in 12 ml of distilled water. Meanwhile, 2.0 mmol of 1,3,5-benzenetricarboxylic acid was dissolved in 12 ml of ethanol. The two solutions were then mixed and transferred to Teflon liners. The prepared stainless-steel bombs containing Teflon vessels were tightly capped and placed in an oven at 110 °C for 18 h. The resulting MOF crystals were filtered and washed 3 times in ethanol, followed by 3 washes with distilled water. The resulting material was then dried at room temperature and activated in a vacuum dryer at 80 °C for 8 h.

Ni-MOF-74 was synthesized in accordance with the procedure described elsewhere (Jodłowski et al. 2020), with some modifications. A total of 2.3 mmol of zinc nitrate hexahydrate and 0.75 mmol of 2,5-dihydroxyterephtalic acid (DHTP) were dissolved in 30 ml of N,N-dimethylformamide. After the metal salt and DHTP were fully dissolved, 1.5 ml of distilled water was added to the solution. The resulting solution was then transferred to Teflon liners. The prepared stainless-steel bombs containing Teflon vessels were tightly capped and placed in an oven at 100 °C for 20 h. The resulting MOF crystals were left in methanol for seven days, with the methanol being replaced with fresh methanol every two days. The resulting material was then dried at room temperature and activated in a vacuum dryer at 180 °C for 6 h.

UiO-66 was synthesized in accordance with the procedure described elsewhere (Jodłowski et al. 2021), with some modifications. A total of 0.082 mmol of zirconium (IV) chloride and 0.78 mmol of benzene-1,4-dicarboxylic acid (H2BDC) was dissolved in 81.7 ml of N,N-dimethylformamide. The resulting mixture was then ultrasonicated for 5 minutes, after which 9.2 ml of acetic acid was added. The resulting solution was then transferred to Teflon liners. The prepared stainless-steel bombs containing Teflon vessels were tightly capped and placed in an oven at 120 °C for 24 h. The resulting MOF crystals were separated from the solution by centrifugation. The white crystals were washed 3 times in DMF, followed by 3 washes with methanol. The material was then dried at room temperature and activated in a vacuum dryer at 120 °C for 12 h.

MIL-140A was synthesized in accordance with the procedure described elsewhere (Jodłowski et al. 2023), with some modifications The sonochemical synthesis of MIL-140A metal–organic frameworks were performed using a two-step approach. In the first step, 2 mmol of zirconium (IV) chloride and 4 mmol of benzene-1,4-dicarboxylic acid (H_2BDC) was suspended in 12 ml of N,N-dimethylformamide. Next, 0.016 ml of hydrochloric acid was added to the suspension. The resulting solution was then transferred to Teflon liners. The prepared stainless-steel bombs containing Teflon vessels were tightly capped and placed in an oven at 220 °C for 20 h. The resulting Pre-MIL-140A crystals were separated from the solution by filtration. The white crystals were washed 3 times with DMF, followed by 3 washes with methanol. The resulting material was then dried at room temperature and activated in a vacuum dryer at 120 °C for 12 h. In the next step, the as-prepared Pre-MIL-140A was further sonicated by using the QSonica Q700 sonicator equipped with a ½" diameter horn. A total of 200 mg of Pre-MIL-140A was suspended in a mixture of 25 ml of methanol and 25 ml of acetic acid. The resulting suspension was placed in an ice bath. The suspension was then treated by sonication for 30 min at an amplitude of 60. Prior to sonication, the suspension was purged with an Ar flow of 50 ml/min for 10 min. The resulting crystals were centrifuged, washed three times with methanol, dried at room temperature, and then activated in a vacuum dryer at 120 ◦C for 10 h.

The successful synthesis of the MOF materials was confirmed by PXRD analysis (Figure 1A). Simulated XRD patterns were also generated based on the literature (Haldoupis et al. 2015, Jodłowski et al. 2023, Sose et al. 2021, Valenzano et al. 2011) (Figure 1B). A comparison of PXRD patterns of the synthesized MOF materials with literature data confirms their high crystallinity (Bordiga et al. 2007, Jodłowski et al. 2020, 2021, 2022, 2023).

Methods

The structure of selected MOF materials was characterized using scanning electron microscopy (SEM) and low-pressure gas adsorption (LPA) analyses. The LPA analyses were performed using a volumetric method on an ASAP 2020 analyzer, with nitrogen (N_2) as the adsorbate at 77 K and an absolute pressure range of 0-100 kPa. Prior to measurement, the samples were degassed under UHV for 12 h at 353 K (Ni-MOF-74), 378 K (MIL-140A) and 423 K (HKUST-1, UiO-66). Based on the equilibrium sorption points, N_2 adsorption isotherms and structural parameters were plotted. The Langmuir single-layer sorption model (Langmuir 1918) and

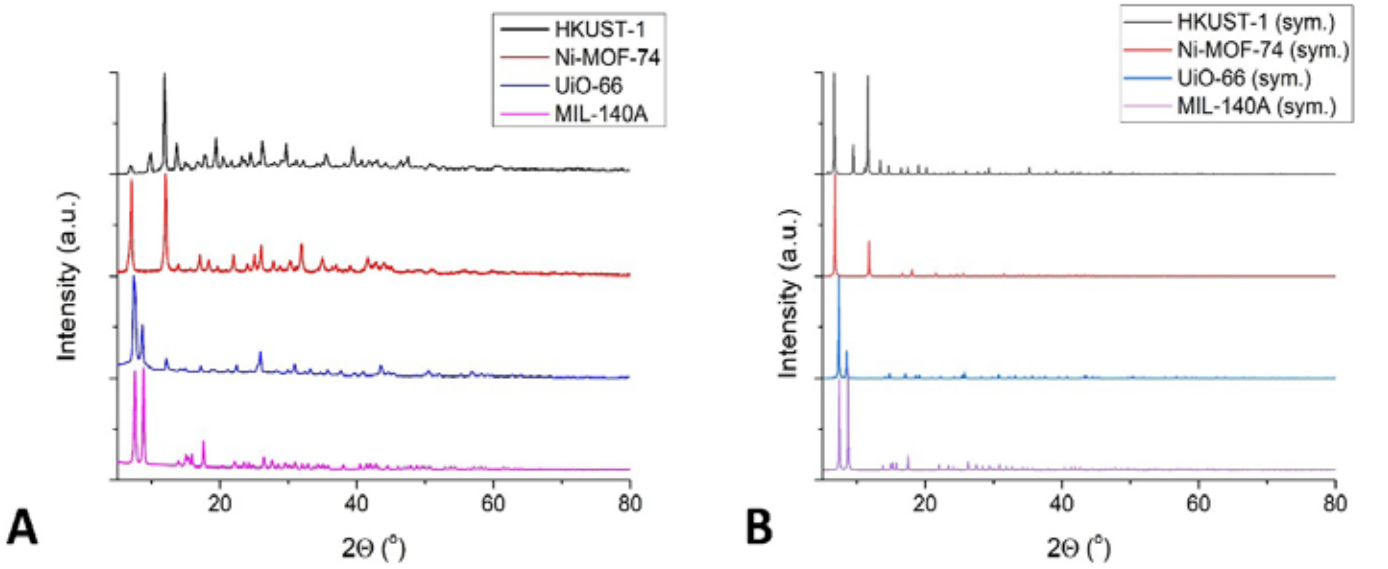

Figure 1. A) PXRD diffraction patterns of synthesized MOF; B) Simulated XRD of the tested MOFs based on (Haldoupis et al. 2015, Jodłowski et al. 2023, Sose et al. 2021, Valenzano et al. 2011)

the BET multilayer adsorption model (Brunauer et al. 1938) were used to determine the structural parameters. The BJH model (Barrett et al. 1951), based on the Kelvin equation, and the DFT model (Olivier 1995), based on density functional theory, were used to characterize the pore size distribution.

Sorption measurements of the MOF materials for CO_2 and CH_4 were carried out using gravimetric method on an IGA-001 analyzer. The analyses were performed at temperatures of 278 K, 293 K, 313 K, 333 K and 353 K, with absolute pressure values of 20 kPa, 40 kPa, 60 kPa, 100 kPa, 200 kPa, 400 kPa, 800 kPa and 1600 kPa. Each sample was degassed in UHV at 353 K for 24 hours before measurement. Based on the obtained sorption points, the sorption isotherms for pure CO_2 and CH_4 were plotted.

Subsequently, the isosteric heat of adsorption was determined using the indirect Clausius-Clapeyron method (Cimino et al. 2017, Giraldo et al. 2019, Nuhnen and Janiak 2020). Each sorption isotherm was described by a function based on the Langmuir-Freundlich model:

$$a = \frac{A_{LF} * (K * p)^n}{1 + (K * p)^n} \quad (1)$$

where: a is the sorption capacity at the measurement temperature and pressure, (mmol/g); A_{LF} is the maximum sorption capacity at the measurement temperature, (mmol/g); K is the adsorption equilibrium constant or affinity constant, (1/kPa); p is the absolute pressure, (kPa); n is the heterogeneity exponent, (-), with a value in the range $0<n\leq1$, where $n = 1$ the corresponds to a Langmuir isotherm.

Using the values of the parameter A_{LF}, the Avogadro number N_A and the sitting area of the CO_2 molecule (ω_{CO_2}), the Langmuir-Freundlich specific surface area values were determined:

$$SSA_{LF} = A_{LF} * N_A * \omega_g \quad (2)$$

where: SSA_{LF} is the specific surface area according to the Langmuir-Freundlich model, (m^2/g); N_A is Avogadro's constant, (1/mmol); ω_g is the sitting area of the gas molecule: CO_2 or CH_4, (m^2).

To determine the thermal effects accompanying the sorption of CO_2 or CH_4 on MOF compounds, the isosteric heat of adsorption was calculated using the Clausius-Clapeyron equation (Myers 2002). This method relies on determining at least two sorption isotherms at different temperatures and fitting them with a mathematical model (in this case, the Langmuir-Freundlich model) to find the pressure values at different temperatures where the same amount of adsorbate is adsorbed (Giraldo et al. 2019, Mason et al. 2014, Sircar et al. 1999). The following assumptions underlie this method: the gas behaves as an ideal gas, and the molar volume of the adsorbed gas is neglected (Chakraborty et al. 2009). After applying these assumptions, the equation takes the following form:

$$Q_{st} = R\left(\frac{d(\ln p)}{d\left(\frac{1}{T}\right)}\right)_a \quad (3)$$

where: Q_{st} is the isosteric heat of adsorption, (kJ/mol); R is the gas constant, (J/(mol*K)); and T is the measurement temperature, (K).

Results

Structural characteristic

The MOFs differ in topology, metal cations, organic ligands, and, as a result, in their overall structure. This diversity is evident in the SEM images (Figure 2). HKUST-1 has a lumped structure with distinct walls, vertices and well-defined edges. These lumps are loosely arranged in relation to each other. Ni-MOF-74 has a vesicular structure, with the vesicles forming conglomerates that adhere closely to one another. In UiO-66, the particles also form conglomerates, creating interconnected spatial structures. MIL-140A, by contrast, consists of small plates with irregular shapes and edges.

Based on the equilibrium adsorption points of the selected MOF structures, the N_2 adsorption isotherms shown in Figure 3A were plotted. These isotherms were classified as type I, according to IUPAC (Thommes et al. 2015).

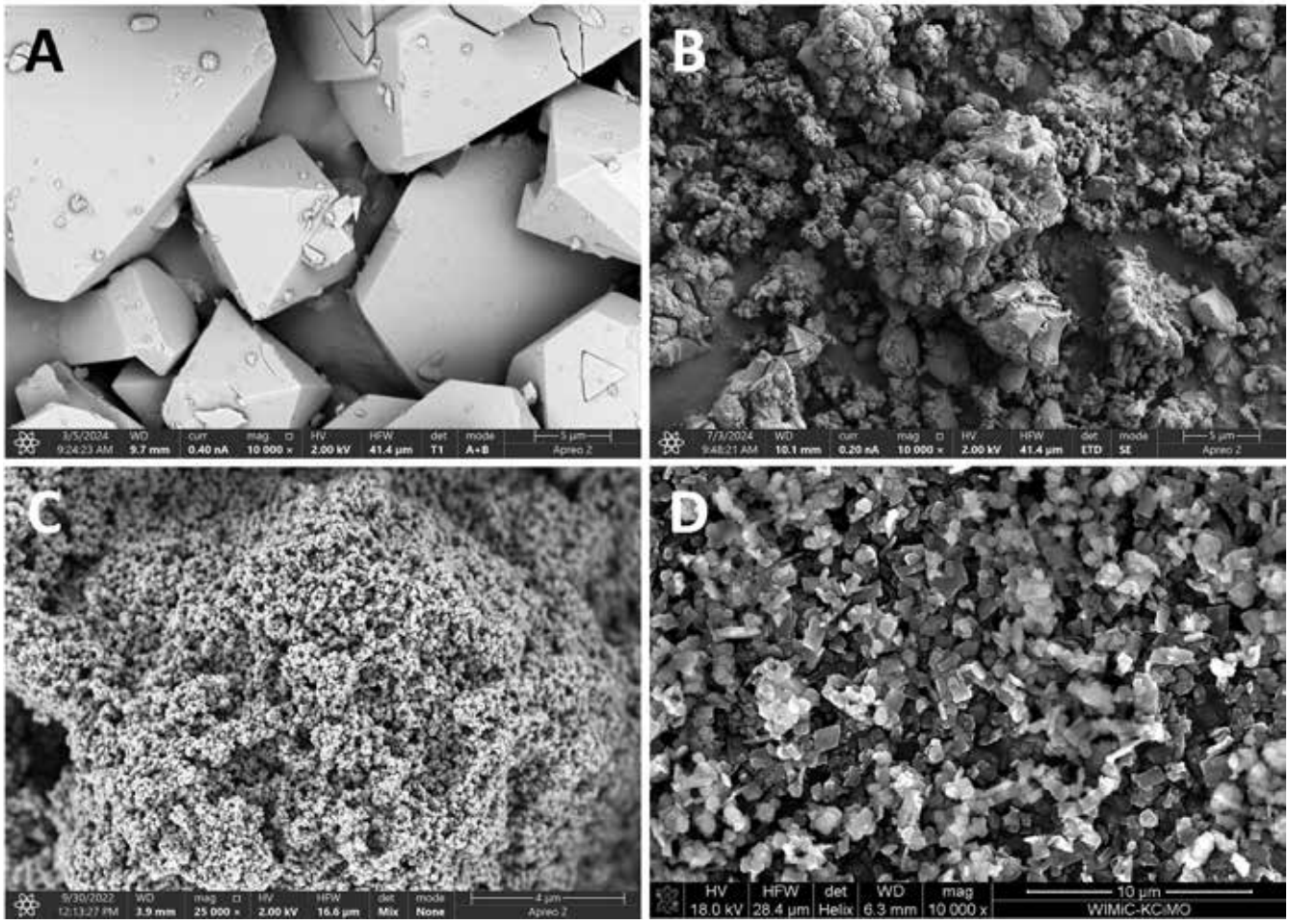

Figure 2. SEM images of A) HKUST-1; B) Ni-MOF-74; C) UiO-66; D) MIL-140A

Based on the N_2 adsorption isotherms, structural parameters were calculated (Table 1). UiO-66 and HKUST-1 had the most extensive pore structures. In UiO-66, the specific surface areas, SSA_{BET} and SSA_L, were 1037 m^2/g and 1468 m^2/g, respectively, while in HKUST-1, they were 1009 m^2/g and 1508 m^2/g, respectively. These MOFs also had the highest total pore volumes (TPV), in terms of both mesopores (TPV_{BJH}) and micropores (TPV_{DFT}). In contrast, Ni-MOF-74 had lower parameter values, with an SSA_{BET} of 685 m^2/g. The lowest values of structural parameters were observed in MIL-140A, which also had the smallest total pore volume (TPV). The pore size distribution, determined using the DFT model (Figure 3B), varied across the MOF structures. Pore diameters ranged from 0.5 to 2 nm, confirming the microporous nature of these

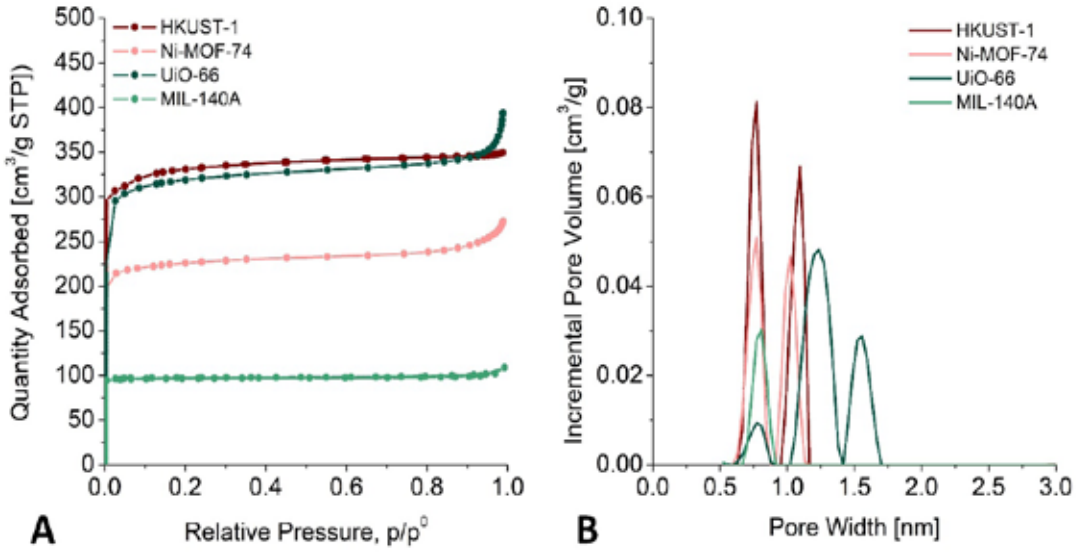

Figure 3. Structural analyses: A) N_2 adsorption isotherms; B) pore size distribution according to the DFT model.

Table 1. Structural parameters

Parameter	A_L	SSA_L	A_{BET}	SSA_{BET}	D_{BJH}	TPV_{BJH}	TPV_{DFT}
Unit	cm³/g STP	m²/g	cm³/g STP	m²/g	nm	cm³/g	cm³/g
HKUST-1	346.41	1507.76	231.82	1009.00	3.00	0.063	0.489
Ni-MOF-74	273.00	1033.46	157.42	685.16	5.85	0.106	0.353
UiO-66	337.25	1467.92	238.35	1037.45	6.40	0.164	0.492
MIL-140A	97.82	425.77	67.95	295.76	10.59	0.023	0.149

where: A_L, A_{BET}, cm³/g - total sorption capacity according to the Langmuir and the BET models; SSA_L, SSA_{BET}, m²/g - specific surface area according to the Langmuir and the BET models; D_{BJH}, nm - average pore diameter according to the BJH model; TPV_{BJH}, TPV_{DFT}, cm³/g - total pore volume according to the BJH model and the DFT model.

materials, as defined by IUPAC (Thommes et al. 2015). In HKUST-1 and Ni-MOF-74, the micropores were finer, with diameters ranging from 0.6 nm to 1.2 nm, while in UiO-66, they ranged from 1.0 nm to 1.7 nm, respectively.

Sorption and heat properties of CO_2 and CH_4

Using gravimetric methods, equilibrium sorption points for CO_2 and CH_4 were determined for the MOFs studied. Based on these data, sorption isotherms described by the Langmuir-Freundlich model were established (Figure 4A-D). Among the tested models, this one provided the best fit to the sorption points in the MOF structures. The MOFs showed higher sorption efficiency for CO_2 compared to CH_4 at each measurement temperature, which is consistent with the literature (Jodłowski et al. 2022). Regardless of the adsorbate type (CO_2, CH_4), the highest values were observed at the lowest temperature of 278

Table 2. CO_2 sorption parameters

Parameter, unit	**278 K**	**293 K**	**313 K**	**333 K**	**353 K**
HKUST-1					
A_{LF}, mmol/g	5.64	5.34	4.99	4.74	5.02
K, 1/kPa	0.0075	0.0051	0.0031	0.0019	0.0010
n, -	0.57	0.63	0.71	0.76	0.76
SSA_{LF}, m²/g	577.6	546.2	510.7	485.1	513.7
Ni-MOF-74					
A_{LF}, mmol/g	10.53	13.90	13.62	12.82	8.52
K, 1/kPa	0.0229	0.0031	0.0016	0.0013	0.0036
n, -	0.54	0.36	0.37	0.43	0.68
SSA_{LF}, m²/g	1077.5	1422.9	1394.2	1312.6	872.0
UiO-66					
A_{LF}, mmol/g	16.96	17.86	14.91	12.23	9.53
K, 1/kPa	0.0010	0.0005	0.0005	0.0005	0.0005
n, -	0.68	0.68	0.74	0.80	0.89
SSA_{LF}, m²/g	1735.8	1828.7	1526.3	1251.5	976.0
MIL-140A					
A_{LF}, mmol/g	2.93	2.81	2.74	2.90	3.15
K, 1/kPa	0.0026	0.0017	0.0009	0.0005	0.0003
n, -	0.83	0.87	0.90	0.91	0.92
SSA_{LF}, m²/g	300.3	287.3	280.6	296.9	322.8

where: A_{LF}, mmol/g - total sorption capacity according to the Langmuir-Freundlich model; K, 1/kPa - the adsorption equilibrium constant; n - the heterogeneity exponent; SSA_{LF}, m²/g - specific surface area according to the Langmuir-Freundlich model.

K and the highest pressure of 1600 kPa. Ni-MOF-74 and UiO-66 exhibited the highest sorption capacities for CO_2, with values ranging from 9 to 10 mmol/g (green lines in Figures 4A-D). In UiO-66, the highest approximated value of A_{LF} sorption capacity at $p \rightarrow \infty$ exceeded 17 mmol/g. In contrast, the sorption capacities for CO_2 in other MOFs were lower, amounting to 5.6 mmol/g (HKUST-1) and 2.9 mmol/g (MIL-140A) (Table 2). CH_4 sorption capacities in all MOFs tested ranged from 1.5 to 5 mmol/g, depending on the type of material tested (purple lines in Figures 4A-D). The highest sorption capacities for CH_4 at 1600 kPa were found in Ni-MOF-74 and UiO-66 MOFs, while the lowest in MIL-140A. The approximate A_{LF} values at $p \rightarrow \infty$ for CH_4 ranged from 2.4 to 9.1 mmol/g and were less dependent on the measurement pressure compared to CO_2 sorption (Table 3).

Based on the equilibrium sorption points, the specific surface area of MOFs relative to CO_2 (SSA_{LF}) was calculated according to equation (2). The degree of surface occupancy of the MOFs by gas particles depended on both the measurement temperature and the type of gas. The SSA_{LF} value was highest at 293 K, with Ni-MOF-74 reaching 1423 m^2/g and UiO-66 reaching 1829 m^2/g. For HKUST-1, the maximum SSA_{LF} value was 578 m^2/g at 278 K, while in MIL-140A, it was 323 m^2/g at 353 K. The calculation results for each temperature are included in Table 2.

The specific surface area relative to methane also depended on the measurement temperature. In Ni-MOF-74 and UiO-66, the values were lower than those observed during carbon dioxide sorption, ranging from 546 to 946 m^2/g. In HKUST-1, the value was similar to that observed for CO_2, while in MIL-140A, it was higher. Table 3 presents the parameter values for CH_4 at all measurement temperatures.

Isosteric heat of adsorption

Conducting sorption measurements at various temperatures allowed for the identification of energy dependencies within the adsorbent (MOF) - adsorbate (CO_2, CH_4) system. These calculations were performed according to equation (3). Isosters were plotted, showing the relationship between ln p and $\frac{1}{T}$ at a constant sorption capacity (a), and the isosteric heat of adsorption values were obtained from the product of the isosteric slope coefficients and R (gas constant).

Figures 5 - 8 show the dependence of the heat released on the degree of surface occupancy of MOF compounds by

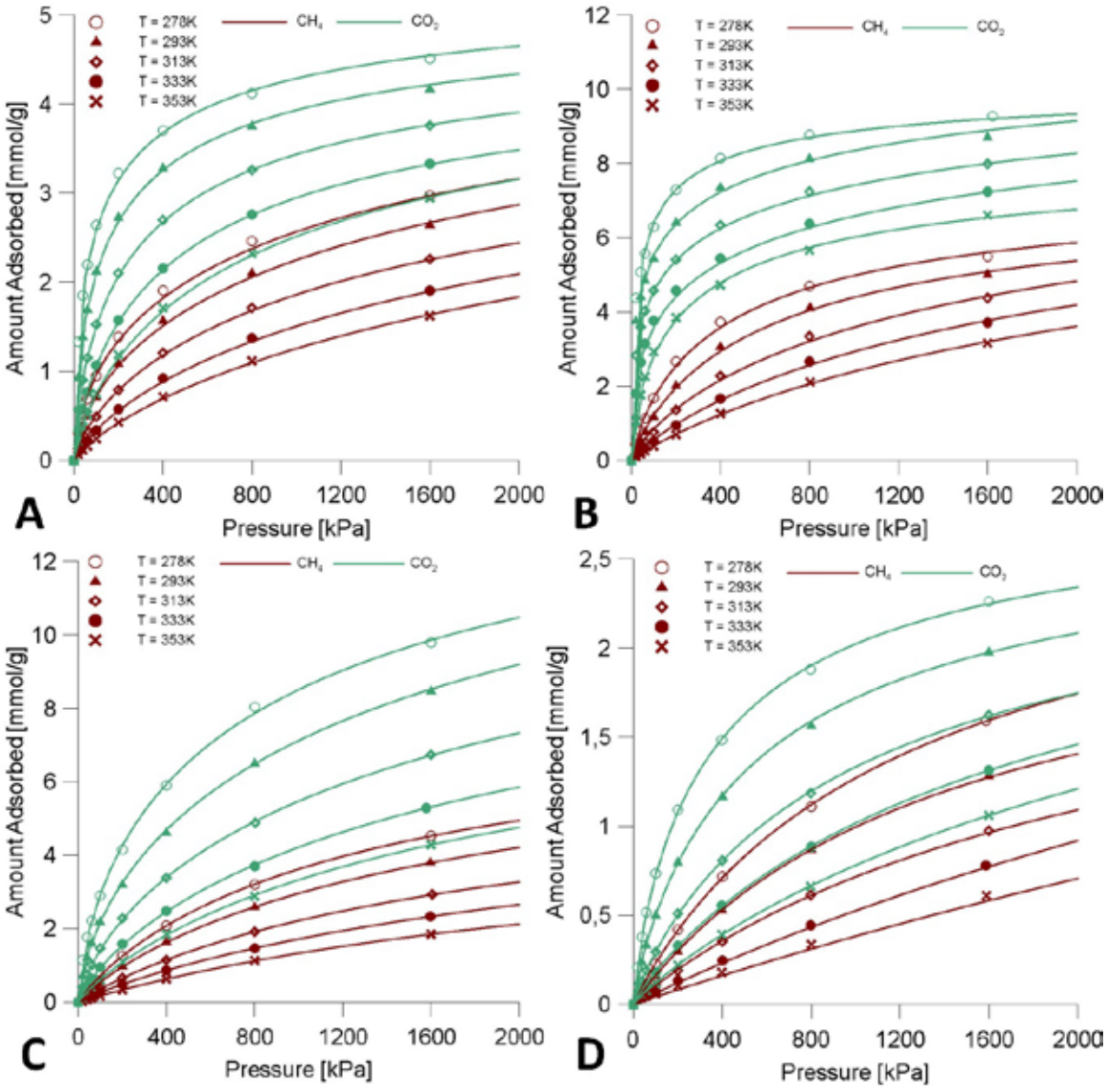

Figure 4. CO_2 and CH_4 adsorption isotherms: A) HKUST-1; B) Ni-MOF-74; C) UiO-66; D) MIL-140A

Table 3. CH_4 sorption parameters

Parameter, unit	**278 K**	**293 K**	**313 K**	**333 K**	**353 K**
HKUST-1					
A_{LF}, mmol/g	5.72	5.48	4.54	4.49	4.63
K, 1/kPa	0.0007	0.0006	0.0006	0.0004	0.0003
n, -	0.61	0.66	0.75	0.79	0.82
SSA_{LF}, m^2/g	595.8	570.5	473.1	467.8	482.4
Ni-MOF-74					
A_{LF}, mmol/g	7.68	7.37	9.08	8.77	8.57
K, 1/kPa	0.0021	0.0016	0.0006	0.0005	0.0004
n, -	0.81	0.87	0.80	0.87	0.91
SSA_{LF}, m^2/g	800.3	767.9	945.7	913.7	892.4
UiO-66					
A_{LF}, mmol/g	8.51	8.20	6.68	6.84	5.24
K, 1/kPa	0.0007	0.0005	0.0005	0.0003	0.0003
n, -	0.90	0.90	0.95	0.92	1.00
SSA_{LF}, m^2/g	886.6	854.1	695.6	712.1	546.2
MIL-140A					
A_{LF}, mmol/g	2.89	2.40	2.38	3.86	4.71
K, 1/kPa	0.0008	0.0007	0.0004	0.0002	0.0001
n, -	0.96	1.00	0.98	0.99	1.00
SSA_{LF}, m^2/g	300.7	250.1	247.7	402.0	490.4

where: A_{LF}, mmol/g - total sorption capacity according to the Langmuir-Freundlich model; K, 1/kPa - the adsorption equilibrium constant; n - the heterogeneity exponent; SSA_{LF}, m^2/g - specific surface area according to the Langmuir-Freundlich model.

carbon dioxide (Figures 5A, 6A, 7A, 8A) and methane (Figures 5B, 6B, 7B, 8B). In most of the MOFs studied, the isosteric heat associated with CO_2 adsorption ranged from about 41-47 kJ/mol at the lowest sorption capacity to 26-30 kJ/mol at the maximum sorption capacity relative to CO_2 (Table 4). Only in MIL-140A were these values notably lower. The changes in the isosteric heat of adsorption with increasing CO_2 particle filling ranged from 5 kJ/mol in MIL-140A (Figure 8A) to 15 kJ/mol in HKUST-1 (Figure 5A). Such a low value indicates the dominant role of dispersion interactions in the CH_4-MOF system.

The thermal effects accompanying methane adsorption were smaller than those observed for carbon dioxide adsorption. The highest value of isosteric heat of adsorption was calculated in HKUST-1, with a maximum of 42 kJ/mol (Table 4). In the other MOFs, the Q_{st}^0 values were lower, ranging from 21-26 kJ/mol. The difference in Q_{st}^0 values between the lowest and highest sorption capacities varied depending on the type of MOF. As the filling of CH_4 molecules increased, the changes ranged from 1.4 kJ/mol in MIL-140A (Figure 8B) to 17 kJ/mol in HKUST-1 (Figure 5B).

Almost all isosteric heat of adsorption curves (Figures 5-8) have a smooth course and indicate energy homogeneity of the adsorbents with respect to CO_2 and CH_4. The exception is the CO_2 adsorption curve for UiO-66 (Figure 7A), where deviations from the trend line of isosteric heat of adsorption of CO_2 are noticeable. These deviations suggest energy inhomogeneity of the adsorbent during CO_2 adsorption.

Table 4. shows the isosteric heat of adsorption (Q_{st}^0) values at "zero occupancy", i.e. at the lowest sorption capacity. Additionally, the thermal selectivity values for the two gases relative to each other Slv_{CO_2/CH_4} were calculated. The highest selectivity of Q_{st}^0 for CO_2 relative to Q_{st}^0 for CH_4 was found in UiO-66 (1.9) and Ni-MOF-74 (1.7). In MIL-140A and HKUST-1, the selectivity values were 1.46 and 1.1, respectively.

Table 4. Isosteric heat of adsorption at lowest sorption capacity and thermal selectivities of CO_2 relative to CH_4

MOF	Q_{st}^0, kJ/mol		Slv_{CO_2/CH_4}, -
	CO_2	CH_4	
HKUST-1	46.66	42.12	1.11
Ni-MOF-74	43.66	25.72	1.70
UiO-66	41.06	21.62	1.90
MIL-140A	31.22	21.39	1.46

where: Q_{st}^0, kJ/mol - isosteric heat of adsorption; Slv_{CO_2/CH_4} - thermal selectivity of CO_2 with respect to CH_4.

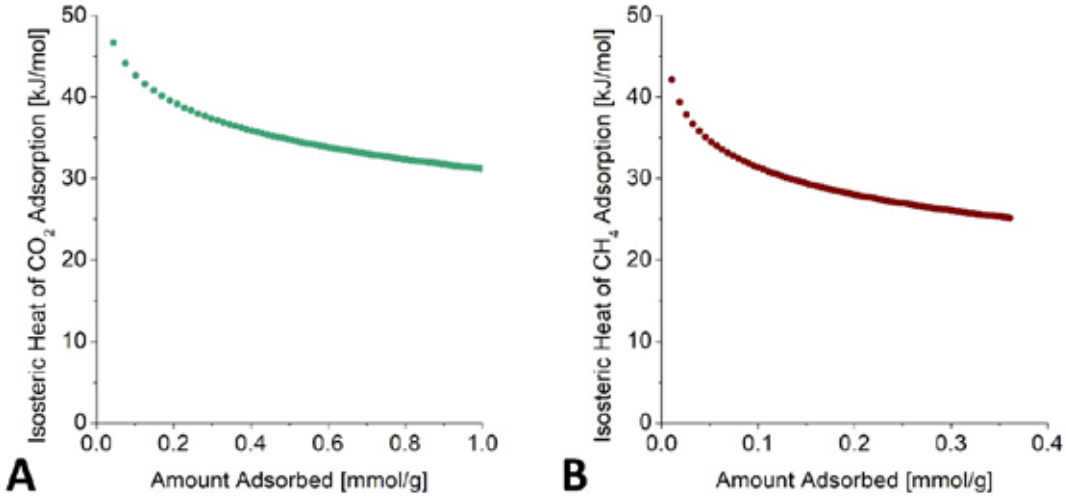

Figure 5. Isosteric heat of adsorption on HKUST-1: A) CO_2 adsorption; B) CH_4 adsorption

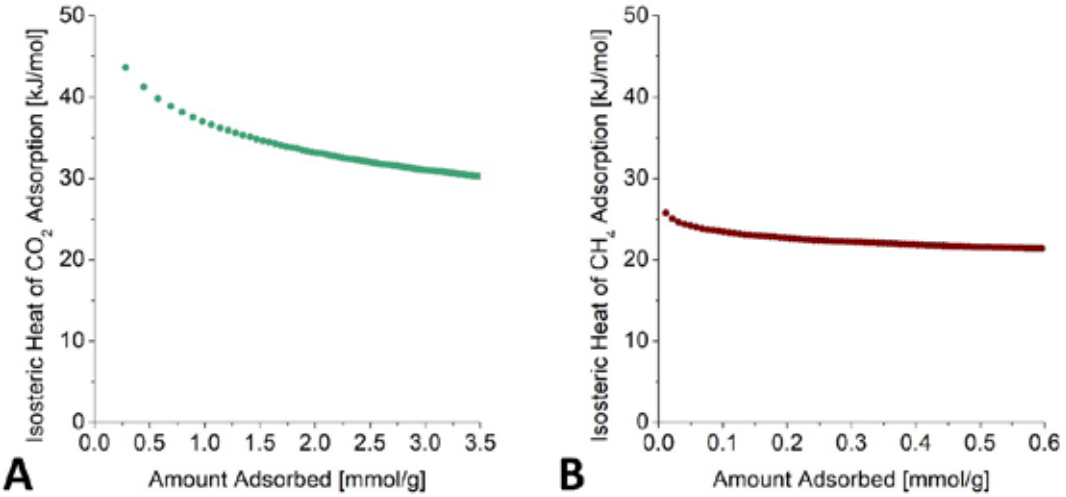

Figure 6. Isosteric heat of adsorption on Ni-MOF-74: A) CO_2 adsorption; B) CH_4 adsorption

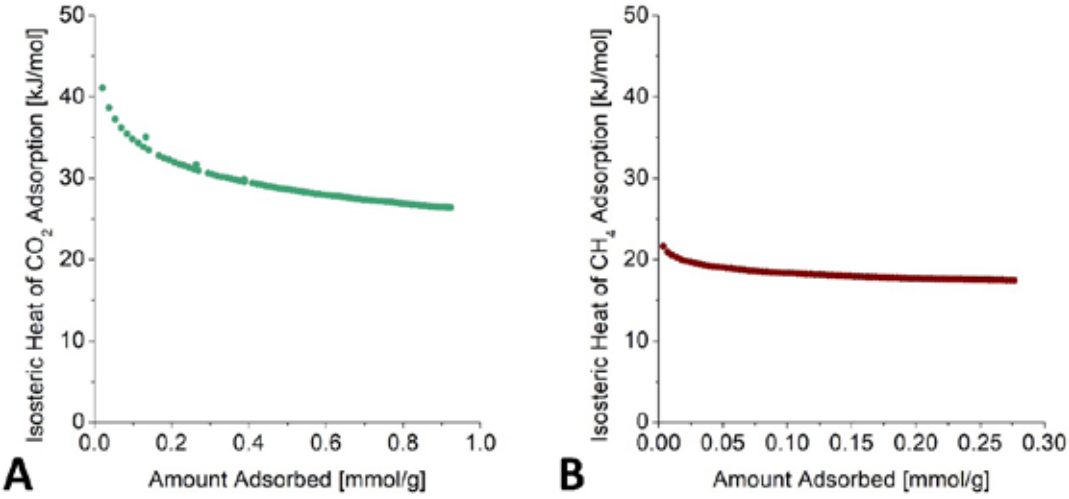

Figure 7. Isosteric heat of adsorption on UiO-66: A) CO_2 adsorption; B) CH_4 adsorption

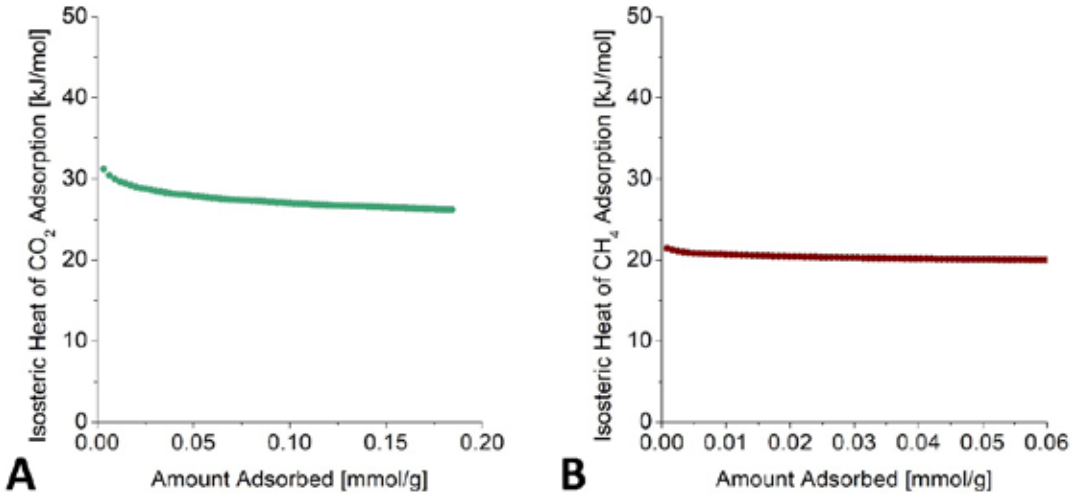

Figure 8. Isosteric heat of adsorption on MIL-140A: A) CO_2 adsorption; B) CH_4 adsorption

Discussion

Four MOFs with different chemical structures and properties were selected for the study; hence the values of structural and sorption parameters determined for them differed. Gas sorption isotherms (CO_2 and CH_4) obtained for these MOFs were characterized as type I isotherms, according to IUPAC (Thommes et al. 2015). The sorption capacities at pressures up to 1600 kPa, as well as the maximum sorption capacity A_{LF} at $p \rightarrow \infty$, were determined. These parameters reached their highest values at the lowest temperature, and their value decreased with increasing temperature, according to the literature (Jodłowski et al. 2022).

In HKUST-1, the maximum sorption capacity A_{LF} relative to CO_2 was 5.6 mmol/g, and the sorption capacity for CH_4 was at a similar level. In the Ni-MOF-74 study, surprising results were obtained, as it was one of the two best MOFs in terms of sorption capacity for both CO_2 and CH_4. Ni-MOF-74 exhibited sorption parameter values twice as high as those of HKUST-1. However, Ni-MOF-74 had lower structural parameter results (SSA_{BET}= 685 m^2/g), while HKUST-1 and UiO-66 had SSA_{BET} values of 1009 m^2/g and 1037 m^2/g, respectively. These structural results indicated that HKUST-1 and UiO-66 had the largest pore space, suggesting the highest sorption potential towards gases.

UiO-66 showed a slightly higher sorption capacity for CO_2 than Ni-MOF-74, with a maximum sorption capacity A_{LF} of 17.0 mmol/g at 278 K. However, in terms of CH_4 adsorption efficiency, UiO-66 was slightly weaker than Ni-MOF-74, as indicated by the shape of the isotherms and the parameters obtained. In MIL-140A, the adsorption efficiencies for CO_2 and CH_4 were approximately two times lower than those of HKUST-1 and about four times lower than those of Ni-MOF-74 and UiO-66. MIL-140A also had the least developed pore space and the lowest values of structural parameters.

The differences in sorption efficiency for CO_2 and CH_4 in the MOFs studied can be attributed to their selective gases sorption. This efficiency depends, among other things, on the kinetic diameter of the gas molecules and the sorption affinity. Since carbon dioxide has a smaller kinetic diameter than methane and a higher sorption affinity in MOFs, it is able to penetrate the finest pores that are inaccessible to methane.

The isosteric heat of adsorption Q_{st}^0 curves for all MOFs followed a pattern typical of microporous adsorbents (Wierzbicki 2019). The highest values of this parameter was observed at the lowest sorption capacities for both CO_2 and CH_4. Energy homogeneity of the adsorbent surface was observed in almost all cases, except during CO_2 adsorption in UiO-66, where this homogeneity was disrupted. The Q_{st}^0 values highlighted structural differences between the studied MOFs, with the values being higher for CO_2 than for CH_4. The highest isosteric heat of adsorption for both CO_2 and CH_4 was calculated for HKUST-1, followed by Ni-MOF-74 and UiO-66, particularly for CO_2 sorption. MIL-140A showed the lowest heat effects. The changes in the isosteric heat of adsorption for CO_2 as the adsorbate loading increased ranged from of 5 to 15 kJ/mol, while for CH_4 they were 1.4-17 kJ/mol, respectively.

Due to the varying Q_{st}^0 values depending on the type of adsorbate, the level of thermal selectivity for CO_2 over CH_4 was determined in the MOFs studied. UiO-66 and Ni-MOF-64 had the highest selectivity, while HKUST-1 had the lowest.

Conclusions

The aim of the research presented was to determine the relationship between the sorption processes of selected GHGs on MOF compounds differing in topology and chemical composition, and their structural properties. Investigating the energetic aspects of sorption is an important part of the methodology for characterizing MOFs structures, enabling qualitative and quantitative analysis of the interactions between them and selected GHGs.

The isosteric heat of adsorption helps clarify the phenomena observed during structural and sorption measurements, addressing uncertainties that often remain unresolved. This was clearly demonstrated with Ni-MOF-74, which, based on structural characterization alone, was expected to perform worse than HKUST-1 and UiO-66 as an adsorbent. However, sorption studies revealed that it was more efficient in GHG accumulation. Without considering the isosteric heat of

adsorption, it would have been impossible to detect the energy inhomogeneity during CO_2 sorption on UiO-66. These results showed that only by obtaining comprehensive structural, sorption and thermal characterization can the properties of the sorbent be fully evaluated.

The work was conducted in the Strata Mechanics Research Institute of the Polish Academy of Sciences and was supported by the Ministry of Science and Higher Education.

References:

Abdelnaby, M. M., Tayeb, I. M., Alloush, A. M., Alyosef, H. A., Alnoaimi, A., Zeama, M., Mohammed, M. G. & Onaizi, S. A. (2024). Post-synthetic modification of UiO-66 analogue metal-organic framework as potential solid sorbent for direct air capture, *Journal of CO2 Utilization*, 79, 102647. DOI:10.1016/j.jcou.2023.102647.

Aniruddha, R., Sreedhar, I. & Reddy, B. M. (2020). MOFs in carbon capture-past, present and future, *Journal of CO2 Utilization*, 42, 101297. DOI:10.1016/j.jcou.2020.101297.

Barrett, E. P., Joyner, L. G. & Halenda, P. P. (1951). The Determination of Pore Volume and Area Distributions in Porous Substances. I. Computations from Nitrogen Isotherms, *Journal of the American Chemical Society*, 73, pp. 373–380. DOI:10.1021/ja01145a126.

Becker, T. M., Heinen, J., Dubbeldam, D., Lin, L.-C. & Vlugt, T. J. H. (2017). Polarizable Force Fields for CO 2 and CH 4 Adsorption in M-MOF-74, *The Journal of Physical Chemistry C*, 121, pp. 4659–4673. DOI:10.1021/acs.jpcc.6b12052.

Bisotti, F., Hoff, K. A., Mathisen, A. & Hovland, J. (2024). Direct Air capture (DAC) deployment: A review of the industrial deployment, *Chemical Engineering Science*, 283, 119416. DOI:10.1016/j.ces.2023.119416.

Bordiga, S., Regli, L., Bonino, F., Groppo, E., Lamberti, C., Xiao, B., Wheatley, P. S., Morris, R. E. & Zecchina, A. (2007). Adsorption properties of HKUST-1 toward hydrogen and other small molecules monitored by IR, *Physical Chemistry Chemical Physics*, 9, 2676. DOI:10.1039/b703643d.

Brunauer, S., Emmett, P. H. & Teller, E. (1938). Adsorption of Gases in Multimolecular Layers, *Journal of the American Chemical Society*, 60, pp. 309–319. DOI:10.1021/ja01269a023.

Canivet, J., Fateeva, A., Guo, Y., Coasne, B. & Farrusseng, D. (2014). Water adsorption in MOFs: fundamentals and applications, *Chem. Soc. Rev.*, 43, pp. 5594–5617. DOI:10.1039/C4CS00078A.

Carreon, M. A. & Venna, S. R. (2020). Metal-Organic Framework Membranes for Molecular Gas Separations, *World Scientific (Europe)*, 6. DOI:10.1142/q0200.

Chai, W., Shen, Y., Wang, J. & Zhang, G. (2022). Applications of Metal-Organic Framework Materials, *Journal of Physics: Conference Series*, 2194, 012014. DOI:10.1088/1742-6596/2194/1/012014.

Chakraborty, A., Saha, B. B., Ng, K. C., Koyama, S. & Srinivasan, K. (2009). Theoretical Insight of Physical Adsorption for a Single-Component Adsorbent + Adsorbate System: I. Thermodynamic Property Surfaces, *Langmuir*, 25, pp. 2204–2211. DOI:10.1021/la803289p.

Choi, I., Jung, Y. E., Yoo, S. J., Kim, J. Y., Kim, H.-J., Lee, C. Y. & Jang, J. H. (2017). Facile Synthesis of M-MOF-74 (M=Co, Ni, Zn) and its Application as an ElectroCatalyst for Electrochemical CO2 Conversion and H2 Production, *Journal of Electrochemical Science and Technology*, 8, pp. 61–68. DOI:10.33961/JECST.2017.8.1.61.

Chowdhury, P., Mekala, S., Dreisbach, F. & Gumma, S. (2012). Adsorption of CO, CO2 and CH4 on Cu-BTC and MIL-101 metal organic frameworks: Effect of open metal sites and adsorbate polarity, *Microporous and Mesoporous Materials*, 152, pp. 246–252. DOI:10.1016/j.micromeso.2011.11.022.

Cimino, R. T., Kowalczyk, P., Ravikovitch, P. I. & Neimark, A. V. (2017). Determination of Isosteric Heat of Adsorption by Quenched Solid Density Functional Theory, *Langmuir*, 33, pp. 1769–1779. DOI:10.1021/acs.langmuir.6b04119.

Czaja, A. U., Trukhan, N. & Müller, U. (2009). Industrial applications of metal–organic frameworks, *Chemical Society Reviews*, 38, 1284. DOI:10.1039/b804680h.

Czarnota, R., Knapik, E., Wojnarowski, P., Janiga, D. & Stopa, J. (2019). Carbon Dioxide Separation Technologies, *Archives of Mining Sciences*, 64, pp. 487–498. DOI:10.24425/ams.2019.129364.

Dhakshinamoorthy, A., Li, Z. & Garcia, H. (2018). Catalysis and photocatalysis by metal organic frameworks, *Chemical Society Reviews*, 47, pp. 8134–8172. DOI:10.1039/C8CS00256H.

Ding, M., Cai, X. & Jiang, H.-L. (2019). Improving MOF stability: approaches and applications, *Chemical Science*, 10, pp. 10209–10230. DOI:10.1039/C9SC03916C

Elhenawy, S. E. M., Khraisheh, M., AlMomani, F. & Walker, G. (2020). Metal-Organic Frameworks as a Platform for CO2 Capture and Chemical Processes: Adsorption, Membrane Separation, Catalytic-Conversion, and Electrochemical Reduction of CO2, *Catalysts*, 10, 1293. DOI:10.3390/catal10111293.

Erans, M., Sanz-Pérez, E. S., Hanak, D. P., Clulow, Z., Reiner, D. M. & Mutch, G. A. (2022). Direct air capture: process technology, techno-economic and socio-political challenges, *Energy & Environmental Science*, 15, pp. 1360–1405. DOI:10.1039/D1EE03523A.

Furukawa, H., Cordova, K. E., O'Keeffe, M. & Yaghi, O. M. (2013). The Chemistry and Applications of Metal-Organic Frameworks, *Science*, 341. DOI:10.1126/science.1230444.

Gargiulo, N., Peluso, A. & Caputo, D. (2020). MOF-Based Adsorbents for Atmospheric Emission Control: A Review, *Processes*, 8, 613. DOI:10.3390/pr8050613.

Giraldo, L., Rodriguez-Estupiñán, P. & Moreno-Piraján, J. C. (2019). Isosteric Heat: Comparative Study between Clausius–Clapeyron, CSK and Adsorption Calorimetry Methods, *Processes*, 7, 203. DOI:10.3390/pr7040203.

Haldoupis, E., Borycz, J., Shi, H., Vogiatzis, K. D., Bai, P., Queen, W. L., Gagliardi, L. & Siepmann, J. I. (2015). Ab Initio Derived Force Fields for Predicting CO 2 Adsorption and Accessibility of Metal Sites in the Metal–Organic Frameworks M-MOF-74 (M = Mn, Co, Ni, Cu), *The Journal of Physical Chemistry C*, 119, pp. 16058–16071. DOI:10.1021/acs.jpcc.5b03700.

Jodłowski, P. J., Kurowski, G., Dymek, K., Jędrzejczyk, R. J., Jeleń, P., Kuterasiński, Ł., Gancarczyk, A., Węgrzynowicz, A., Sawoszczuk, T. & Sitarz, M. (2020). In situ deposition of M(M=Zn; Ni; Co)-MOF-74 over structured carriers for cyclohexene oxidation - Spectroscopic and microscopic characterization, *Microporous and Mesoporous Materials*, 303, 110249. DOI:10.1016/j.micromeso.2020.110249.

Jodłowski, P. J., Kurowski, G., Dymek, K., Oszajca, M., Piskorz, W., Hyjek, K., Wach, A., Pajdak, A., Mazur, M., Rainer, D. N., Wierzbicki, D., Jeleń, P. & Sitarz, M. (2023). From crystal phase mixture to pure metal-organic frameworks – Tuning pore and structure properties, *Ultrasonics Sonochemistry*, 95, 106377. DOI:10.1016/j.ultsonch.2023.106377.

Jodłowski, P. J., Kurowski, G., Kuterasiński, Ł., Sitarz, M., Jeleń, P., Jaśkowska, J., Kołodziej, A., Pajdak, A., Majka, Z. & Boguszewska-Czubara, A. (2021). Cracking the Chloroquine Conundrum: The Application of Defective UiO-66 Metal–Organic Framework Materials to Prevent the Onset of Heart Defects—In Vivo and In Vitro, *ACS Applied Materials & Interfaces*, 13, pp. 312–323. DOI:10.1021/acsami.0c21508.

Jodłowski, P. J., Kurowski, G., Skoczylas, N., Pajdak, A., Kudasik, M., Jędrzejczyk, R. J., Kuterasiński, Ł., Jeleń, P., Sitarz, M., Li, A. & Mazur, M. (2022). Silver and copper modified zeolite imidazole frameworks as sustainable methane storage systems, *Journal of Cleaner Production*, 352, 131638. DOI:10.1016/j.jclepro.2022.131638.

Kong, X.-J. & Li, J.-R. (2021). An Overview of Metal–Organic Frameworks for Green Chemical Engineering, *Engineering*, 7, pp. 1115–1139. DOI:10.1016/j.eng.2021.07.001.

Krzywanski, J., Grabowska, K., Sosnowski, M., Zylka, A., Kulakowska, A., Czakiert, T., Sztekler, K., Wesolowska, M. & Nowak, W. (2022). Heat Transfer in Adsorption Chillers with Fluidized Beds of Silica Gel, Zeolite, and Carbon Nanotubes, *Heat Transfer Engineering*, 43, 172–182. DOI:10.1080/01457632.2021.1874174.

Kurzydym, I. & Czekaj, I. (2020). Modelling of porous metal-organic framework (MOF) materials used in catalysis, *Technical Transactions*, pp. 1–24. DOI:10.37705/TechTrans/e2020012.

Langmuir, I. (1918). THE ADSORPTION OF GASES ON PLANE SURFACES OF GLASS, MICA AND PLATINUM, *Journal of the American Chemical Society*, 40, pp. 1361–1403. DOI:10.1021/ja02242a004.

Lee, Y.-R., Kim, J. & Ahn, W.-S. (2013). Synthesis of metal-organic frameworks: A mini review, *Korean Journal of Chemical Engineering*, 30, pp. 1667–1680. DOI:10.1007/s11814-013-0140-6.

Li, D., Chen, L., Liu, G., Yuan, Z., Li, B., Zhang, X. & Wei, J. (2021). Porous metal–organic frameworks for methane storage and capture: status and challenges, *New Carbon Materials*, 36, pp. 468–496. DOI:10.1016/S1872-5805(21)60034-3.

Li, H., Li, L., Lin, R.-B., Zhou, W., Zhang, Z., Xiang, S. & Chen, B. (2019). Porous metal-organic frameworks for gas storage and separation: Status and challenges, *EnergyChem*, 1, 100006. DOI:10.1016/j.enchem.2019.100006.

Li, M., Zhang, G., Boakye, A., Chai, H., Qu, L. & Zhang, X. (2021). Recent Advances in Metal-Organic Framework-Based Electrochemical Biosensing Applications, *Frontiers in Bioengineering and Biotechnology*, 9. DOI:10.3389/fbioe.2021.797067.

Lin, R.-B., Xiang, S., Xing, H., Zhou, W. & Chen, B. (2019). Exploration of porous metal–organic frameworks for gas separation and purification, *Coordination Chemistry Reviews*, 378, pp. 87–103. DOI:10.1016/j.ccr.2017.09.027.

Madden, D. G., O'Nolan, D., Chen, K.-J., Hua, C., Kumar, A., Pham, T., Forrest, K. A., Space, B., Perry, J. J., Khraisheh, M. & Zaworotko, M. J. (2019). Highly selective CO2 removal for one-step liquefied natural gas processing by physisorbents, *Chemical Communications*, 55, pp. 3219–3222. DOI:10.1039/C9CC00626E.

Mahdipoor, H. R., Halladj, R., Ganji Babakhani, E., Amjad-Iranagh, S. & Sadeghzadeh Ahari, J. (2021). Synthesis, characterization, and CO 2 adsorption properties of metal organic framework Fe-BDC, *RSC Advances*, 11, pp. 5192–5203. DOI:10.1039/D0RA09292D.

Mangal, S., Priya, S. S., Lewis, N. L. & Jonnalagadda, S. (2018). Synthesis and characterization of metal organic framework-based photocatalyst and membrane for carbon dioxide conversion, *Materials Today: Proceedings*, 5, pp. 16378–16389. DOI:10.1016/j.matpr.2018.05.134.

Mason, J. A., Veenstra, M. & Long, J. R. (2014). Evaluating metal–organic frameworks for natural gas storage, *Chem. Sci.*, 5, pp. 32–51. DOI:10.1039/C3SC52633J.

Myers, A. L. (2002). Thermodynamics of adsorption in porous materials, *AIChE Journal*, 48, pp. 145–160. DOI:10.1002/aic.690480115.

Naghdi, S., Shahrestani, M. M., Zendehbad, M., Djahaniani, H., Kazemian, H. & Eder, D. (2023). Recent advances in application of metal-organic frameworks (MOFs) as adsorbent and catalyst in removal of persistent organic pollutants (POPs), *Journal of Hazardous Materials*, 442, 130127. DOI:10.1016/j.jhazmat.2022.130127.

Neimark, A. V., Ravikovitch, P. I., Grün, M., Schüth, F. & Unger, K. K. (1998). Pore Size Analysis of MCM-41 Type Adsorbents by Means of Nitrogen and Argon Adsorption, *Journal of Colloid and Interface Science*, 207, pp. 159–169. DOI:10.1006/jcis.1998.5748.

Nuhnen, A. & Janiak, C. (2020). A practical guide to calculate the isosteric heat/enthalpy of adsorption via adsorption isotherms in metal–organic frameworks, MOFs, *Dalton Transactions*, 49, pp. 10295–10307. DOI:10.1039/D0DT01784A.

Olivier, J. P. (1995). Modeling physical adsorption on porous and nonporous solids using density functional theory, *Journal of Porous Materials*, 2, pp. 9–17. DOI:10.1007/BF00486565.

Olivier, J. P. (2000). Comparison of the experimental isosteric heat of adsorption of argon on mesoporous silica with density functional theory calculations, *Studies in Surface Science and Catalysis*, 128, pp. 81–87. DOI:10.1016/S0167-2991(00)80011-7.

Oschatz, M. & Antonietti, M. (2018). A search for selectivity to enable CO2 capture with porous adsorbents, *Energy & Environmental Science*, 11, pp. 57–70. DOI:10.1039/C7EE02110K.

Pajdak, A., Skoczylas, N., Dębski, A., Grzegorek, J., Maziarz, W. & Kudasik, M. (2019). CO2 and CH4 sorption on carbon nanomaterials and coals – Comparative characteristics, *Journal of Natural Gas Science and Engineering*, 72, 103003. DOI:10.1016/j.jngse.2019.103003.

Park, H. J. & Suh, M. P. (2013). Enhanced isosteric heat, selectivity, and uptake capacity of CO2 adsorption in a metal-organic framework by impregnated metal ions, *Chem. Sci.*, 4, pp. 685–690. DOI:10.1039/C2SC21253F.

Park, K. S., Ni, Z., Côté, A. P., Choi, J. Y., Huang, R., Uribe-Romo, F. J., Chae, H. K., O'Keeffe, M. & Yaghi, O. M. (2006). Exceptional chemical and thermal stability of zeolitic imidazolate frameworks, *Proceedings of the National Academy of Sciences*, 103, pp. 10186–10191. DOI:10.1073/pnas.0602439103.

Qazvini, O. T., Babarao, R. & Telfer, S. G. (2021). Selective capture of carbon dioxide from hydrocarbons using a metal-organic framework, *Nature Communications*, 12, 197. DOI:10.1038/s41467-020-20489-2.

Qian, Q., Asinger, P. A., Lee, M. J., Han, G., Mizrahi Rodriguez, K., Lin, S., Benedetti, F. M., Wu, A. X., Chi, W. S. & Smith, Z. P. (2020). MOF-Based Membranes for Gas Separations, *Chemical Reviews*, 120, pp. 8161–8266. DOI:10.1021/acs.chemrev.0c00119.

Rafati Jolodar, A., Abdollahi, M., Fatemi, S. & Mansoubi, H. (2024). Enhancing carbon dioxide separation from natural gas in dynamic adsorption by a new type of bimetallic MOF;

MIL-101(Cr-Al), *Separation and Purification Technology*, 334, 125990. DOI:10.1016/j.seppur.2023.125990.

Rieth, A. J., Wright, A. M. & Dincă, M. (2019). Kinetic stability of metal–organic frameworks for corrosive and coordinating gas capture, *Nature Reviews Materials*, 4, pp. 708–725. DOI:10.1038/s41578-019-0140-1.

Senkovska, I. & Kaskel, S. (2008). High pressure methane adsorption in the metal-organic frameworks Cu3(btc)2, Zn2(bdc)2dabco, and Cr3F(H2O)2O(bdc)3, *Microporous and Mesoporous Materials*, 112, pp. 108–115. DOI:10.1016/j.micromeso.2007.09.016.

Sircar, S., Mohr, R., Ristic, C. & Rao, M. B. (1999). Isosteric Heat of Adsorption: Theory and Experiment, *The Journal of Physical Chemistry B*, 103, pp. 6539–6546. DOI:10.1021/jp9903817.

Sose, A. T., Cornell, H. D., Gibbons, B. J., Burris, A. A., Morris, A. J. & Deshmukh, S. A. (2021). Modelling drug adsorption in metal–organic frameworks: the role of solvent, *RSC Advances*, 11, pp. 17064–17071. DOI:10.1039/D1RA01746B.

Strauss, I., Mundstock, A., Treger, M., Lange, K., Hwang, S., Chmelik, C., Rusch, P., Bigall, N. C., Pichler, T., Shiozawa, H. & Caro, J. (2019). Metal–Organic Framework Co-MOF-74-Based Host–Guest Composites for Resistive Gas Sensing, *ACS Applied Materials & Interfaces*, 11, pp. 14175–14181. DOI:10.1021/acsami.8b22002.

Thommes, M., Kaneko, K., Neimark, A. V., Olivier, J. P., Rodriguez-Reinoso, F., Rouquerol, J. & Sing, K. S. W. (2015). Physisorption of gases, with special reference to the evaluation of surface area and pore size distribution (IUPAC Technical Report), *Pure and Applied Chemistry*, 87, pp. 1051–1069. DOI:10.1515/pac-2014-1117.

Tlili, N., Grévillot, G. & Vallières, C. (2009). Carbon dioxide capture and recovery by means of TSA and/or VSA, *International Journal of Greenhouse Gas Control*, 3, pp. 519–527. DOI:10.1016/j.ijggc.2009.04.005.

Valenzano, L., Civalleri, B., Chavan, S., Bordiga, S., Nilsen, M. H., Jakobsen, S., Lillerud, K. P. & Lamberti, C. (2011). Disclosing the Complex Structure of UiO-66 Metal Organic Framework: A Synergic Combination of Experiment and Theory, *Chemistry of Materials*, 23, pp. 1700–1718. DOI:10.1021/cm1022882.

Valverde, A., G.-Sainz, P., Orive, J., Larrea, E., Reizabal-Para, A., Tovar, G., Copello, G., Lázaro-Martinez, J. M., Rodriguez, B., Gonzalez-Navarrete, B., Quintero, Y., Rosales, M., García, A., Arriortua, M. I. & Fernández de Luis, R. (2021). Chapter Three - Porous, lightweight, metal organic materials: environment sustainability, in: Advanced Lightweight Multifunctional Materials, Costa, P., Costa, C. M., Lanceros-Mendez, S. (Eds.). *Woodhead Publishing*, pp. 49-129. DOI:10.1016/B978-0-12-818501-8.00012-3.

Wierzbicki, M. (2019). Izosteryczne ciepło sorpcji metanu na wybranych węglach kamiennych, *PRZEMYSŁ CHEMICZNY*, 1, pp. 139–143. DOI:10.15199/62.2019.4.22.

Xiao, T. & Liu, D. (2019). The most advanced synthesis and a wide range of applications of MOF-74 and its derivatives, *Microporous and Mesoporous Materials*, 283, pp. 88–103. DOI:10.1016/j.micromeso.2019.03.002.

Xu, B., Zhang, H., Mei, H. & Sun, D. (2020). Recent progress in metal-organic framework-based supercapacitor electrode materials, *Coordination Chemistry Reviews*, 420, 213438. DOI:10.1016/j.ccr.2020.213438.

Yulia, F., Utami, V. J., Nasruddin, N. & Zulys, A. (2019). Synthesis, Characterizations, and Adsorption Isotherms of CO2 on Chromium Terephthalate (MIL-101) Metal-organic Frameworks (MOFs), *International Journal of Technology*, 10, 1427. DOI:10.14716/ijtech.v10i7.3706.

Zhou, J., Zeng, C., Ou, H., Yang, Q., Xie, Q., Zeb, A., Lin, X., Ali, Z. & Hu, L. (2021). Metal–organic framework-based materials for full cell systems: a review, *Journal of Materials Chemistry C*, 9, pp. 11030–11058. DOI:10.1039/D1TC01905H.

Zylka, A., Krzywanski, J., Czakiert, T., Idziak, K., Sosnowski, M., de Souza-Santos, M. L., Sztekler, K. & Nowak, W. (2020). Modeling of the Chemical Looping Combustion of Hard Coal and Biomass Using Ilmenite as the Oxygen Carrier, *Energies*, 13, 5394. DOI:10.3390/en13205394.

Adsorpcja wybranych gazów cieplarnianych na związkach metaloorganicznych MOF w kontekście towarzyszących jej efektów cieplnych

Streszczenie. Efekty termiczne towarzyszące sorpcji gazu na materiałach mikro- i mezoporowatych dostarczają unikalnych spostrzeżeń na temat rodzaju, przebiegu i efektywności sorpcji. W niniejszym artykule zsyntetyzowano i zbadano związki metaloorganiczne (MOF) o skrajnie różnej topografii i budowie chemicznej: HKUST-1, Ni-MOF-74, UiO-66 i MIL-140A. MOFy te scharakteryzowano strukturalnie i sorpcyjnie względem wybranych GHG. Określono pojemności sorpcyjne względem CO_2 i CH_4 w kilku temperaturach i ciśnieniach pomiaru oraz określono maksymalną pojemność sorpcyjną zgodnie z modelem Langmuira-Freundlicha. Wyznaczono efekty cieplne towarzyszące adsorpcji poprzez parametr izosterycznego ciepła sorpcji. Dla każdego z MOFów wartości izosterycznego ciepła adsorpcji były wyższe względem CO_2, niż względem CH_4. Wartości tego parametru określono w następującej kolejności: HKUST-1 > Ni-MOF-74 > UiO-66 > MIL-140A. W prawie każdym przypadku zaobserwowano jednorodność energetyczną powierzchni adsorbentu, poza UiO-66 podczas adsorpcji CO_2. Zmiany wyznaczonego izosterycznego ciepła sorpcji CO_2 wraz ze wzrostem pojemności sorpcyjnej były w zakresie 5-15 kJ/mol, natomiast względem CH_4 wyniosły odpowiednio 1.4-17 kJ/mol. Określono poziom selektywności cieplnej CO_2 względem CH_4. Najwyższą selektywność posiadały UiO-66 (1.9) oraz Ni-MOF-74 (1.7), natomiast najniższą MIL-140A (1.5) i HKUST-1 (1.1).